Kelvin Probe Force Microscopy by Dissipative Electrostatic Force Modulation

Yoichi Miyahara,[*] Jessica Topple, Zeno Schumacher, and Peter Grutter

Department of Physics, Faculty of Science, McGill University, Montreal, Quebec, Canada H3A 2T8

(Received 25 August 2015; revised manuscript received 29 October 2015; published 23 November 2015)

We report an experimental technique for Kelvin probe force microscopy using the dissipation signal of frequency-modulation atomic force microscopy for bias-voltage feedback. It features a simple implementation and faster scanning as it requires no low-frequency modulation. The dissipation is caused by the oscillating electrostatic force that is coherent with the tip oscillation, which is induced by a sinusoidally oscillating voltage applied between the tip and sample. We analyze the effect of the phase of the oscillating force on the frequency shift and dissipation and found that the relative phase of 90° that causes only the dissipation is the most appropriate for Kelvin-probe-force-microscopy measurements. The present technique requires a significantly smaller ac-voltage amplitude by virtue of enhanced force detection due to the resonance enhancement and the use of fundamental flexural-mode oscillation for electrostatic force detection. This feature will be of great importance in the electrical characterizations of technically relevant materials whose electrical properties are influenced by the externally applied electric field as is the case in semiconductor electronic devices.

DOI: 10.1103/PhysRevApplied.4.054011

I. INTRODUCTION

Kelvin probe force microscopy (KPFM), a variant of atomic force microscopy (AFM) has become one of the indispensable tools used to investigate electronic properties of nanoscale material as well as nanoscale devices. In KPFM, a surface potential of a sample is measured by detecting a capacitive electrostatic force that is a function of the surface potential and applied bias voltage. In order to separate the electrostatic force component from other force components such as the van der Waals force, chemical bonding force, and magnetic force, the electrostatic force is modulated by applying an ac bias voltage and the resulting modulated component of the measured force is detected by lock-in detection [1].

KPFM has been implemented in a variety of ways that can be classified into two distinct categories, amplitude modulation (AM) [2–4] and frequency modulation (FM) [4,5]. The former implementation takes advantage of enhanced electrostatic force-detection sensitivity by tuning the modulation frequency to one of the resonance frequencies of the AFM cantilever, leading to an enhanced detection of the electrostatic force by its quality (Q) factor that can reach over 10 000 in vacuum [6].

The latter method (FM KPFM) detects the modulation in the resonance frequency shift that is induced by a low-frequency ac voltage. While this method requires a much higher ac-voltage amplitude, it offers higher spatial resolution because the resonance frequency shift is determined by the electrostatic force gradient with respect to the tip-sample distance rather than the force itself [3,4,7].

Here, we report a KPFM implementation (D KPFM) using the dissipation signal of conventional FM-AFM systems to detect the electrostatic force. The dissipation arises from an oscillating electrostatic force acting on the AFM tip that is coherent with the tip oscillation (trajectory). The oscillating electrostatic force is induced by applying an ac voltage between the tip and sample. By setting the phase of the ac voltage to 90° out of phase with respect to the tip oscillation, an electrically induced dissipation can result without affecting the resonance frequency shift, allowing topography imaging to be performed in constant frequency-shift mode. The KPFM feedback loop can be implemented with the electrically induced dissipation signal as it is proportional to the effective dc potential difference between the tip and sample $(V_{\mathrm{bias}} - V_{\mathrm{CPD}})$, where V_{bias} and V_{CPD} are an applied dc voltage and the contact potential difference, respectively.

This technique makes it possible to take full advantage of the enhanced force sensitivity by the high Q-factor fundamental resonance mode, as there is no need to excite higher flexural modes for the electrostatic force detection. In conventional AM KPFM [2,3], because the fundamental mode is used for topography imaging, the frequency of ac bias voltage is typically configured to excite a higher resonance mode (typically second flexural mode) that has a much higher effective spring constant as well as lower quality factor [8], canceling the resonance enhancement. The enhanced sensitivity of the technique presented here allows the use of a much smaller ac voltage enabling less invasive potential measurements, which is of great importance in the electrical characterizations of technically

[*]Corresponding author.
yoichi.miyahara@mcgill.ca

 © 2015 American Physical Society

relevant materials whose electrical properties are influenced by the externally applied electric field as is the case in semiconductor electronic devices.

Although a similar technique has already been reported by Fukuma *et al.* [9], it has not been adopted widely, probably because of the complexity in its implementation. The present technique is simpler in implementation and even requires no additional lock-in amplifier, as there is no low-frequency modulation involved.

II. THEORY

The electrostatic force between two conductors connected to an ac and dc voltage source F_{elec} is described as follows [10]:

$$\begin{aligned} F_{\mathrm{elec}} &= \frac{1}{2}\frac{\partial C}{\partial z}\{V_{\mathrm{bias}} - V_{\mathrm{CPD}} + V_{\mathrm{ac}}\cos(\omega_{\mathrm{el}}t + \phi)\}^2 \\ &= \alpha\{V_{\mathrm{dc}} + V_{\mathrm{ac}}\cos(\omega_{\mathrm{el}}t + \phi)\}^2 \\ &= F_0 + F_1 + F_2 \\ \alpha &\equiv \frac{1}{2}\frac{\partial C}{\partial z}, \\ V_{\mathrm{dc}} &\equiv V_{\mathrm{bias}} - V_{\mathrm{CPD}}, \end{aligned} \tag{1}$$

where C is the tip-sample capacitance, V_{bias} and V_{CPD} are the applied dc voltage and the contact potential difference, and V_{ac}, ω_{el}, and ϕ are the amplitude, angular frequency, and phase of the ac bias voltage. z is the position of the tip with respect to the sample surface and the oscillating tip around its mean position z_0, expressed as $z(t) = z_0 + A\cos(\omega_m t)$, with ω_m and A being its oscillation angular frequency and amplitude, respectively. We assume that the tip oscillation is driven by another means such as piezoacoustic or photothermal excitation and its frequency $f_m = \omega_m/2\pi$ is chosen to be that of the fundamental flexural resonance mode f_0.

Expanding Eq. (1) and isolating each harmonic component, F_0, F_1, and F_2, which result from the applied ac bias voltage, yields the following terms:

$$F_0 = \alpha\left(V_{\mathrm{dc}}^2 + \frac{V_{\mathrm{ac}}^2}{2}\right), \tag{2}$$

$$F_1 = 2\alpha V_{\mathrm{dc}} V_{\mathrm{ac}}\cos(\omega_{\mathrm{el}}t + \phi), \tag{3}$$

$$F_2 = \frac{1}{2}\alpha V_{\mathrm{ac}}^2\cos\{2(\omega_{\mathrm{el}}t + \phi)\}. \tag{4}$$

Notice that the z dependence of $\alpha = \frac{1}{2}(\partial C/\partial z)(z)$ must be taken into account in order to correctly describe the response of the oscillating cantilever subject to the oscillating electrostatic force induced by the coherent ac voltage.

By expanding α around the mean position z_0, and taking the first order term, α is expressed as follows [11]:

$$\alpha(z) \approx \alpha(z_0) + \alpha'(z - z_0) = \alpha_0 + \alpha' A\cos(\omega_m t). \tag{5}$$

Substituting Eq. (5) into Eq. (2) and rearranging, it yields

$$\begin{aligned} F_0(t) &= \{\alpha_0 + \alpha' A\cos(\omega_m t)\}\left(V_{\mathrm{dc}}^2 + \frac{V_{\mathrm{ac}}^2}{2}\right) \\ &= \alpha_0\left(V_{\mathrm{dc}}^2 + \frac{V_{\mathrm{ac}}^2}{2}\right) + \alpha' A\left(V_{\mathrm{dc}}^2 + \frac{V_{\mathrm{ac}}^2}{2}\right)\cos(\omega_m t). \end{aligned} \tag{6}$$

Note that the second term expresses an oscillating force whose frequency is $\omega_m/2\pi$ while the first term expresses the static deflection of the cantilever. As this oscillating force is in phase with respect to $z(t)$, it results in a shift in resonance frequency [12].

Substituting Eq. (5) into the expression of F_1 [Eq. (3)] gives

$$\begin{aligned} F_1(t) &= 2\{\alpha_0 + \alpha' A\cos(\omega_m t)\}V_{\mathrm{dc}}V_{\mathrm{ac}}\cos(\omega_{\mathrm{el}}t + \phi) \\ &= 2\alpha_0 V_{\mathrm{dc}}V_{\mathrm{ac}}\cos(\omega_{\mathrm{el}}t + \phi) \\ &\quad + \alpha' A V_{\mathrm{dc}}V_{\mathrm{ac}}[\cos\{(\omega_{\mathrm{el}} + \omega_m)t + \phi)\} \\ &\quad + \cos\{(\omega_{\mathrm{el}} - \omega_m)t - \phi\}]. \end{aligned} \tag{7}$$

We focus on a special case where $\omega_{\mathrm{el}} = \omega_m$. $F_1(t)$ can be simplified as follows:

$$\begin{aligned} F_1(t) &= \alpha' A V_{\mathrm{dc}}V_{\mathrm{ac}}\cos\phi + 2\alpha_0 V_{\mathrm{dc}}V_{\mathrm{ac}}\cos(\omega_m t + \phi) \\ &\quad + \alpha' A V_{\mathrm{dc}}V_{\mathrm{ac}}\cos(2\omega_m t + \phi). \end{aligned} \tag{8}$$

We notice that the interaction between the mechanical oscillation of the tip and the oscillating electrostatic force produce a static force and two harmonic forces with frequency ω_m and $2\omega_m$.

Likewise, $F_2(t)$ [Eq. (4)] contains three harmonic terms with their frequency, ω_m, $2\omega_m$, and $3\omega_m$ under the same condition ($\omega_m = \omega_{\mathrm{el}}$) as follows:

$$\begin{aligned} F_2(t) &= \frac{1}{2}\{\alpha_0 + \alpha' A\cos(\omega_m t)\}V_{\mathrm{ac}}^2\cos\{2(\omega_{\mathrm{el}}t + \phi)\} \\ &= \frac{1}{2}\alpha_0 V_{\mathrm{ac}}^2\cos\{2(\omega_m t + \phi)\} \\ &\quad + \frac{1}{4}\alpha' A V_{\mathrm{ac}}^2\{\cos(\omega_m t + 2\phi) + \cos(3\omega_m t + 2\phi)\}. \end{aligned} \tag{9}$$

As is shown in the theory of FM-AFM [12–14], the resonance frequency shift and dissipation signal are essentially determined by the in-phase and quadrature component of the fundamental harmonic component (in this case

ω_m) of the oscillating force, respectively. Putting together all the ω_m components from F_0, F_1, and F_2 and rearranging them, we get the following expression:

$$F_\omega(t) = F_{\rm in}\cos\omega_m t + F_{\rm quad}\sin\omega_m t, \tag{10}$$

where

$$F_{\rm in} = \alpha' A\left(V_{\rm dc} + \frac{\alpha_0\cos\phi}{\alpha' A}V_{\rm ac}\right)^2 \tag{11}$$

$$-\left[\frac{\alpha_0^2\cos^2\phi}{\alpha' A} - \frac{\alpha' A}{2}\left(1+\frac{\cos 2\phi}{2}\right)\right]V_{\rm ac}^2, \tag{12}$$

$$F_{\rm quad} = -2\alpha_0 V_{\rm dc}V_{\rm ac}\sin(\phi) - \frac{1}{2}\alpha' A V_{\rm ac}^2\sin(\phi)\cos(\phi). \tag{13}$$

These $F_{\rm in}$ and $F_{\rm quad}$ cause the resonance frequency shift and dissipation signal in FM-AFM, respectively. As can be seen in the formula for $F_{\rm in}$, the frequency shift versus $V_{\rm dc}$ curve will be a parabola whose minimum is shifted from $V_{\rm CPD}$ by the value determined by the phase ϕ and amplitude $V_{\rm ac}$ of the oscillating bias voltage. This indicates that the bias voltage at the parabola minimum is no longer $V_{\rm CPD}$. However, in the special case where $\phi = 90°$, we find

$$F_{\rm in} = \alpha' A\left(V_{\rm dc}^2 + \frac{V_{\rm ac}^2}{4}\right), \tag{14}$$

$$F_{\rm quad} = -2\alpha_0 V_{\rm dc}V_{\rm ac} = -2\alpha_0(V_{\rm bias} - V_{\rm CPD})V_{\rm ac}. \tag{15}$$

The resulting resonance frequency shift Δf and the dissipation signal g are obtained using the formulas found in Refs. [12–14] as follows:

$$\Delta f = -\frac{1}{2}\frac{f_0}{k}\frac{F_{\rm in}}{A} = -\frac{1}{2}\frac{f_0}{k}\alpha'\left\{(V_{\rm bias} - V_{\rm CPD})^2 + \frac{V_{\rm ac}^2}{4}\right\}, \tag{16}$$

$$g = g_0\left(1 - \frac{Q}{kA}F_{\rm quad}\right) = g_0\left\{1 + 2\frac{Q}{kA}\alpha_0(V_{\rm bias} - V_{\rm CPD})V_{\rm ac}\right\}, \tag{17}$$

where k is the effective spring constant of the fundamental flexural mode of the cantilever and g_0 is the dissipation without the ac bias voltage which is given by the mechanical Q factor of the cantilever. In the case where the applied bias $V_{\rm bias}$ is equal to the contact potential difference $V_{\rm CPD}$, the dissipation goes back to its original value g_0. It is therefore possible to use the dissipation signal g as the KPFM bias-voltage feedback signal with g_0 as its control setpoint value. We notice that the frequency shift is proportional to the electrostatic force gradient, whereas the dissipation signal is proportional to the electrostatic force and Q/k, which is the case for AM KPFM.

III. EXPERIMENT

Figure 1 depicts the block diagram of the experimental setup used for D-KPFM measurements. As we notice, the D-KPFM technique requires only two additional components, a phase shifter and proportional-integrator (PI) controller compared to normal FM-AFM systems. The fundamental flexural-mode oscillation of the AFM cantilever is controlled by a self-oscillation feedback loop electronics which consists of a phase shifter and an amplitude controller. The amplitude controller is used to maintain a constant oscillation amplitude and composed of a root-mean-square (rms) amplitude detector and a PI controller (NanoSurf easyPLLplus oscillator controller). The output of the amplitude feedback PI controller is the dissipation signal which will be used for controlling the dc bias voltage. The detection bandwidth of the rms amplitude detector is extended to about 1 kHz by replacing the integration capacitor in the original rms detector circuit.

The deflection signal is fed into the additional phase shifter, which serves to adjust the relative phase ϕ to produce the ac voltage which is 90° out of phase to the cantilever deflection. Because of the phase delay in the deflection sensing electronics, the actual phase-shift value set by the phase shifter may be different from 90°. The dissipation signal acts as the input signal to the PI controller, which adjusts the applied dc bias $V_{\rm bias}$ to maintain a constant dissipation equal to the value without $V_{\rm ac}$ applied, g_0.

We use a JEOL JSPM-5200 atomic force microscope for the experiments with the modifications described below. The original laser diode is replaced by a fiber-optic collimator with a focusing lens that is connected to a fiber-coupled laser diode module (OZ Optics). The laser diode is mounted on a temperature-controlled fixture and its driving current is

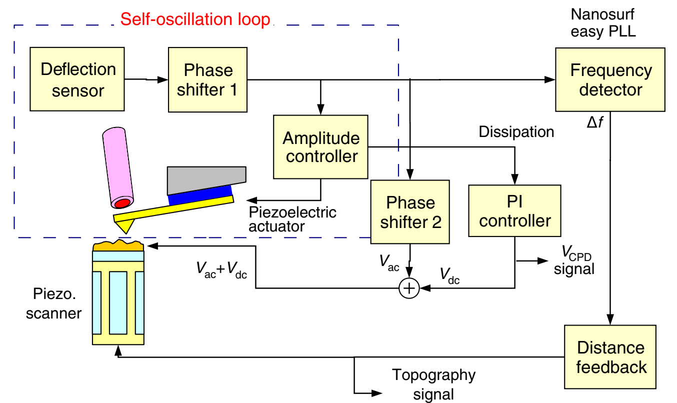

FIG. 1. Block diagram of the experimental setup for D-KPFM measurements.

modulated with a radio-frequency signal to reduce the deflection detection noise [15]. The bias voltage is applied to the sample with reference to the grounded AFM tip to reduce the effect of the capacitive crosstalk of V_{ac} to the piezoelectric actuator used for cantilever excitation [16,17]. The piezoelectric actuator is shunted with a chip resistor with low resistance (∼10 Ω) to further reduce the effect. The original controller is replaced with an open-source controller GXSM [18] with the dedicated acquisition hardware (MK2-A810, SoftdB).

Commercial silicon AFM cantilevers (NSC15, MikroMasch) with a typical spring constant of ∼20 N/m and resonance frequency of ∼300 kHz are used in a high-vacuum environment with the pressure of $\sim 5 \times 10^{-7}$ mbar.

IV. RESULTS AND DISCUSSION

Figure 2 shows simultaneously measured Δf and g versus V_{bias} curves with a coherent sinusoidally oscillating voltage with the amplitude $V_{ac} = 100\ \mathrm{mV}_{p\text{-}p}$ and various phase ϕ. The curves are taken on a Si substrate with a 200-nm-thick oxide SiO_2. A fitted curve with a parabola for Δf-V_{bias} curves [Eq. (12)] or a linear line for g-V_{bias} curves [Eq. (13)] is overlaid on each experimental curve, indicating a very good agreement between the theory and experiments. As can be seen in Figs. 2(a) and 2(b), the position of the parabola vertex shifts and the slope of the g-V_{bias} curve changes systematically with varying phase.

In order to further validate the theoretical analysis, the voltage for the parabola maximum of the Δf-V_{bias} curves and the slope of the g-V_{bias} curves are plotted against the phase ϕ in Fig. 3. Each plot is overlaid with a fitted curve (solid curve) with the cosine function [Eq. (12)] for the parabola maximum and with the sine function [Eq. (13)] for the dissipation slope, demonstrating an excellent agreement between the experiment and theory. The voltage for the parabola maximum versus the phase curve intersects the value for the parabola without ac bias voltage at the phase of 97° as opposed to 90°, which is predicted by the theory. This deviation is mainly due to the phase delay in the photodiode preamplifer electronics. The dissipation slope takes its maximum value at around 81°, again deviating from the theoretical value of 90°. This deviation is probably due to the residual capacitive crosstalk to the piezoelectric actuator [16,17].

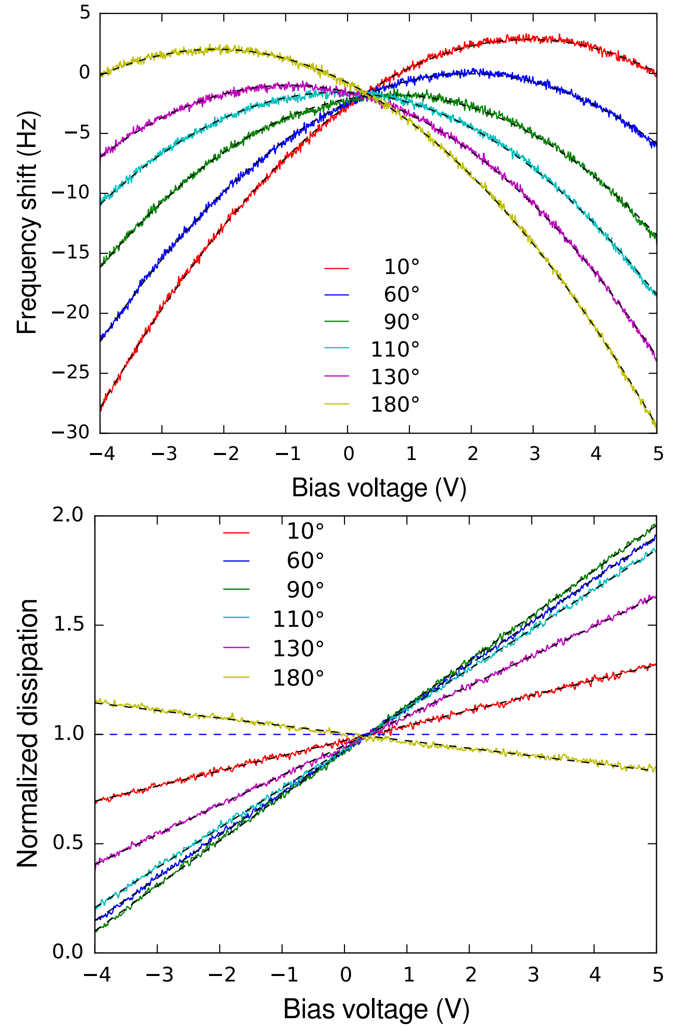

FIG. 2. (a) Frequency shift Δf and (b) dissipation signal g versus dc bias voltage V_{bias} curves taken with a coherent sinusoidally oscillating voltage with the amplitude $V_{ac} = 100\ \mathrm{mV}_{p\text{-}p}$ and various phases ϕ applied to a 200-nm-thick SiO_2-on-Si substrate. The dissipation signal is normalized with the value without the ac bias voltage (indicated with the horizontal blue dashed line). In both figures, each of the dashed lines represent fitted curves assuming a parabola for Δf and a linear line for g as indicated in Eqs. (12) and (13), respectively. The oscillation amplitude of the tip is 7.2 $\mathrm{nm}_{p\text{-}p}$ and the quality factor of the cantilever is 9046.

Figure 4 shows topography and potential images of a patterned MoS_2 on the 200-nm-thick SiO_2/Si substrate taken by (a) D-KPFM, (b) AM-KPFM, and (c) FM-KPFM techniques. The D-KPFM and FM-KPFM images are taken with the same cantilever tip (resonance frequency, 306 553 Hz; spring constant, 20.8 N/m; quality factor, 14 963), and the AM-KPFM image is taken with a different one (resonance frequency, 298044 Hz; spring constant, 27.2 N/m; quality factor, 14 700). These two cantilevers are of the same type and taken from the same batch. In D-KPFM imaging, a sinusoidally oscillating voltage with an amplitude of $V_{ac} = 100\ \mathrm{mV}_{p\text{-}p}$ phase locked with the tip oscillation is applied to the sample. In AM-KPFM imaging, a sinusoidally oscillating voltage with an amplitude of $V_{ac} = 8\ \mathrm{V}_{p\text{-}p}$ whose frequency is tuned to the second flexural resonance peak (resonance frequency, 1 903 500 Hz; quality factor, 2400) is applied to the sample. The resulting oscillation amplitude is detected by a high-speed lock-in amplifier (HF2LI, Zurich Instruments) and used for the dc bias-voltage feedback [2,3]. In FM-KPFM imaging, a sinusoidally oscillating voltage with the amplitude of $V_{ac} = 2.0\ \mathrm{V}_{p\text{-}p}$

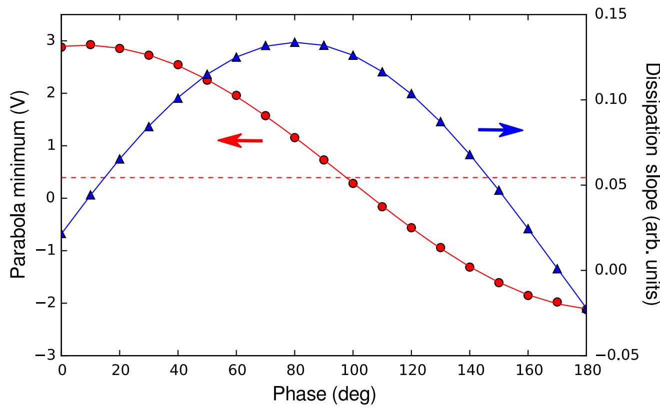

FIG. 3. Voltage of minimum of the measured Δf-$V_{\rm bias}$ curves (red circles) [Fig. 2(a)] and the slope of dissipation-$V_{\rm bias}$ curves (blue circles) [Fig. 2(b)]. Each solid line represents the fitted curve with the cosine function [Eq. (12)] for the parabola minimum and with the sine function [Eq. (13)] for the dissipation slope. The horizontal dashed line indicates the voltage for parabola minimum without the ac bias voltage.

and frequency of 300 Hz is applied to the sample. The number of pixels in the images is 512×512. The scanning time for D-KPFM, AM-KPFM, and FM-KPFM imaging are 2 s/line, resulting in the total scanning time of 1024 s/frame. In all the imaging modes, the frequency-shift signal is used for topography feedback.

A flake of MoS_2 is deposited onto a SiO_2/Si substrate by mechanical exfoliation and a stripe pattern is created by reactive ion etching on the top of the flake. The topography images show an unetched ridge located between the etched regions. The height of the ridge is approximately 20 nm with respect to the etched regions. A clear fractal-like pattern can be seen on the ridge in all of the potential images. The potential contrast can be ascribed to the residue of the etch resist (PMMA) as the topography images show the similar contrast whose thickness is about 1 nm.

When comparing the potential images taken by D KPFM [Fig. 4(a)] and AM KPFM [Fig. 4(b)], the D-KPFM potential image shows better clarity than that by AM KPFM. The difference is due to the lower signal-to-noise ratio of the amplitude signal of the second flexural-mode oscillation even though a much higher $V_{\rm ac} = 8\ {\rm V}_{p\text{-}p}$ is applied in AM KPFM. The higher (~40 times higher than the first mode [19]) effective spring constant and lower observed quality factor (2400 compared with 14 700 for the first mode) account for the difference as the signal in both operating modes is proportional to Q/k. Figure 4(d) shows the line profiles of potential on the same location indicated in the potential images as a white line. Two profiles are in a very good agreement, indicating the similarity of D KPFM and AM KPFM, both of which are sensitive to the electrostatic force. The constant offset between two profiles is probably due to the different tips used in the two separate experiments.

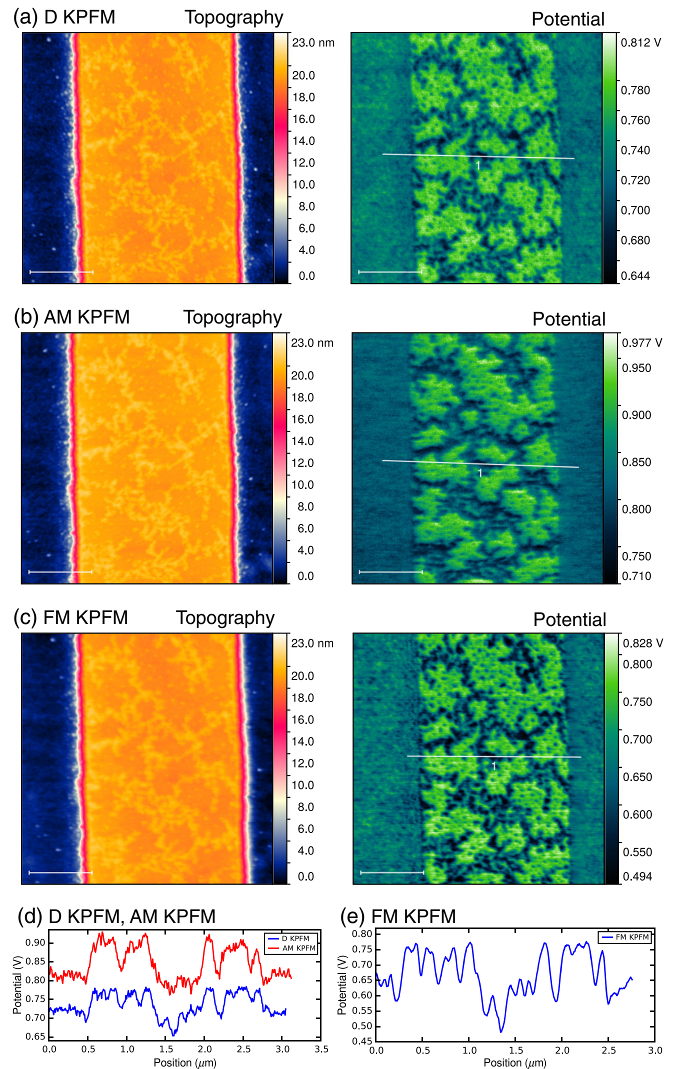

FIG. 4. Simultaneously taken topography (left) and potential (right) images of patterned MoS_2 on a SiO_2/Si substrate by (a) D-KPFM techniques ($\Delta f = -10.3$ Hz, $A = 6.2\ {\rm nm}_{p\text{-}p}$, $V_{\rm ac} = 100\ {\rm mV}_{p\text{-}p}$), (b) AM-KPFM techniques ($\Delta f = -13.4$ Hz, $A = 16\ {\rm nm}_{p\text{-}p}$, $V_{\rm ac} = 8\ {\rm V}_{p\text{-}p}$, $f_{\rm ac} = 1903\,500$ Hz), and (c) FM-KPFM techniques ($\Delta f = -7.0$ Hz, $A = 7\ {\rm nm}_{p\text{-}p}$, $V_{\rm ac} = 2.0\ {\rm V}_{p\text{-}p}$, $f_{\rm ac} = 300$ Hz). (d) Line profiles of the D-KPFM (blue) and AM-KPFM (red) potential images. (e) Line profile of the FM-KPFM potential image. The scale bar is 1 μm.

Although both potential images taken with D KPFM and FM KPFM show a very similar pattern on the ridge with the nearly same clarity, we notice a lower contrast in the potential image taken with D KPFM than that with FM KPFM from the inspection of the line profiles (Figs. 4(d) and (e)). The peak-to-peak value of the potential variation in the D-KPFM image is ~0.12 V, about one-half that in the FM-KPFM image (~0.3 V). The similar difference in the potential contrast taken with FM KPFM and AM KPFM has also been reported in the literature and is ascribed to the fact that the AM KPFM is sensitive to electrostatic force, whereas FM KPFM uses the modulation

in the resonance frequency shift which is sensitive to force gradient [4,20]. The similarity between D KPFM and AM KPFM is apparent in the expression of g [Eq. (17)] which is proportional to $\alpha_0 = \frac{1}{2}(\partial C/\partial z)|_{z_0}$ rather than α'. This indicates that the smaller potential contrast observed in D KPFM resulted from a larger spatial average due to the stray capacitance including the body of the tip and the cantilever [21–24].

In spite of lower potential contrast, D KPFM has a clear advantage in that it requires much smaller $V_{\mathrm{ac}} = 100$ mV$_{p\text{-}p}$ compared with 1 V$_{p\text{-}p}$ for FM KPFM and 8 V$_{p\text{-}p}$ for AM KPFM. This advantage is important for such samples as a semiconductor where the influence of the large V_{ac} can be very important due to band-bending effects.

The detection bandwidth of D KPFM is determined by the bandwidth of the amplitude-control feedback loop used in FM AFM. In fact, applying the coherent V_{ac} causing dissipative force can be used to measure the dynamics of the amplitude-control feedback system. In FM AFM, the AFM cantilever serves for the frequency-determining element of an oscillator circuit (i.e., self-oscillator) so that the oscillation frequency of the oscillator keeps track of the resonance frequency of the cantilever. In this way, the conservative force has no influence on the drive amplitude [25,26] and the amplitude controller compensates for the effective Q factor change caused by dissipative force. Therefore, by modulating V_{bias} at a low frequency ($<$ a few kHz) together with applying the coherent V_{ac}, the amplitude of the dissipative force can be modulated as can been seen in Eq. (15) and the frequency response of the amplitude feedback loop can thus be measured with a lock-in amplifier. The measured -3 dB bandwidth of the amplitude feedback loop is as high as 1 kHz, which is wider than that of the phase locked loop (PLL) frequency detector (400 Hz). Note that in contrast to the settling time of the oscillation amplitude of a cantilever subject to a change in conservative force which is $\tau \sim Q/f_0$ [26], the amplitude response time to a dissipative force is not limited by Q and can be faster because of the active damping mechanism built in the amplitude-control feedback loop [27] as well as the induced energy dissipation which is given by $\pi F_{\mathrm{quad}} A$ in addition to the internal dissipation of the cantilever, $\pi k A^2/Q$. This explains the observed fast response of the amplitude feedback loop, resulting in the wider bandwidth of the voltage feedback loop in D KPFM than that in FM KPFM that is limited by PLL demodulation bandwidth (typically < 1 kHz) which sets the bias modulation frequency.

The noise of V_{CPD} is ultimately determined by the noise in the tip oscillation amplitude δA. The change in the oscillation amplitude of the self-excited cantilever ΔA, caused by the dissipative force F_{quad}, is given by

$$\Delta A = -\frac{Q}{k} F_{\mathrm{quad}} = -\frac{Q}{k} \alpha_0 V_{\mathrm{dc}} V_{\mathrm{ac}} = \frac{Q}{k} \frac{\partial C}{\partial z}\bigg|_{z_0} V_{\mathrm{dc}} V_{\mathrm{ac}}. \quad (18)$$

Equation (18) resembles the amplitude response of a simple harmonic oscillator driven on resonance on which AM KPFM is based.

The noise in V_{CPD}, δV_{CPD} can thus be expressed as follows:

$$\delta V_{\mathrm{CPD}} = \frac{k}{Q} \frac{\delta A}{\frac{\partial C}{\partial z}\big|_{z_0} V_{\mathrm{ac}}}, \quad (19)$$

which agrees with the result by Fukuma *et al.* [9]. This indicates that δV_{CPD} is proportional to k/Q. The source of δA can be either detector noise or thermal noise depending on the particular AFM system and its operating condition. More detailed discussion on the noise in AM KPFM is found in the literature [28]. In typical AM-KPFM measurements [20] where the second flexural-mode oscillation is used for detecting electrostatic force, the improvement of δV_{CPD} by the enhanced Q factor is partially canceled by the substantially higher dynamic spring constant and lower quality factor of the second mode as we have demonstrated in Fig. 4. D KPFM enables us to fully take advantage of the resonance enhancement while retaining the advantages of the single-pass FM-AFM.

So far, we assumed that no other process other than the dissipative electrostatic force causes the dissipation signal in FM-AFM systems. Although it is often the case that the contributions from other processes are negligible, even when other intrinsic [29,30] or extrinsic [25] dissipation processes are present, it is possible to separate the electrostatic dissipation induced by F_{quad} just as is done in FM KPFM with Δf. In this case V_{bias} needs to be modulated at a low frequency and the resulting modulated dissipation signal is used for the dc bias feedback. Clearly, this scheme is slower than the fast response achieved by the D-KPFM technique.

V. CONCLUSION

In conclusion, we report an experimental technique for Kelvin probe force microscopy using the dissipation signal of FM-AFM for dc voltage feedback. It features the simpler implementation and faster scanning as it requires no low-frequency modulation. The dissipation is caused by the oscillating electrostatic force that is coherent with the tip oscillation, which is induced by a sinusoidally oscillating ac voltage applied between the tip and sample. We analyzed the effect of the phase of the oscillating force on the frequency shift and dissipation and found that the relative phase of 90° is the most appropriate for KPFM measurements. The D-KPFM technique requires a significantly smaller ac-voltage amplitude (a few tens of mV) by virtue of the resonance enhanced force detection and the use of fundamental flexural-mode oscillation. This feature will be useful in the electrical characterizations of materials whose electrical properties are sensitive to the externally applied electric field.

ACKNOWLEDGMENTS

The authors would like to thank Dr. Omid Salehzadeh Einabad and Professor Zetian Mi at McGill University for providing the MoS_2 sample. This work was partly supported by the Natural Science and Engineering Research Council (NSERC), le Fonds Québécois de Recherche sur la Nature et les Technologies (FQRNT).

[1] M. Nonnenmacher, M. P. O'Boyle, and H. K. Wickramasinghe, Kelvin probe force microscopy, Appl. Phys. Lett. **58**, 2921 (1991).

[2] A. Kikukawa, S. Hosaka, and R. Imura, Vacuum compatible high-sensitive Kelvin probe force microscopy, Rev. Sci. Instrum. **67**, 1463 (1996).

[3] Ch. Sommerhalter, Th. W. Matthes, Th. Glatzel, A. Jäger-Waldau, and M. Ch. Lux-Steiner, High-sensitivity quantitative Kelvin probe microscopy by noncontact ultra-high-vacuum atomic force microscopy, Appl. Phys. Lett. **75**, 286 (1999).

[4] U. Zerweck, C. Loppacher, T. Otto, S. Grafstrom, and L. M. Eng, Accuracy and resolution limits of Kelvin probe force microscopy, Phys. Rev. B **71**, 125424 (2005).

[5] S. Kitamura, K. Suzuki, and M. Iwatsuki, High resolution imaging of contact potential difference using a novel ultrahigh vacuum non-contact atomic force microscope technique, Appl. Surf. Sci. **140**, 265 (1999).

[6] Z. Schumacher, Y. Miyahara, L. Aeschimann, and P. Grütter, Improved atomic force microscopy cantilever performance by partial reflective coating, Beilstein J. Nanotechnol. **6**, 1450 (2015).

[7] S. A. Burke, J. M. LeDue, Y. Miyahara, J. M. Topple, S. Fostner, and P. Grutter, Determination of the local contact potential difference of PTCDA on NaCl: A comparison of techniques, Nanotechnology **20**, 264012 (2009).

[8] O. Pfeiffer, C. Loppacher, C. Wattinger, M. Bammerlin, U. Gysin, M. Guggisberg, S. Rast, R. Bennewitz, E. Meyer, and H.-J. Güntherodt, Using higher flexural modes in non-contact force microscopy, Appl. Surf. Sci. **157**, 337 (2000).

[9] T. Fukuma, K. Kobayashi, H. Yamada, and K. Matsushige, Surface potential measurements by the dissipative force modulation method, Rev. Sci. Instrum. **75**, 4589 (2004).

[10] L. N. Kantorovich, A. I. Livshits, and M. Stoneham, Electrostatic energy calculation for the interpretation of scanning probe microscopy experiments, J. Phys. Condens. Matter **12**, 795 (2000).

[11] When the higher order terms are included, α' in Eq. (5) needs to be replaced with a linear combination of higher order derivatives (only odd number terms). However, Eq. (5) itself still remains in the same form, which means that the main result, Eq. (15), is still rigorously valid as the contribution of the derivatives do not come into Eq. (15) when $\phi = 90°$.

[12] H. Hölscher, B. Gotsmann, W. Allers, U. D. Schwarz, H. Fuchs, and R. Wiesendanger, Measurement of conservative and dissipative tip-sample interaction forces with a dynamic force microscope using the frequency modulation technique, Phys. Rev. B **64**, 075402 (2001).

[13] L. N. Kantorovich and T. Trevethan, General Theory of Microscopic Dynamical Response in Surface Probe Microscopy: From Imaging to Dissipation, Phys. Rev. Lett. **93**, 236102 (2004).

[14] J. E. Sader, T. Uchihashi, M. J. Higgins, A. Farrell, Y. Nakayama, and S. P. Jarvis, Quantitative force measurements using frequency modulation atomic force microscopy—Theoretical foundations, Nanotechnology **16**, S94 (2005).

[15] T. Fukuma, M. Kimura, K. Kobayashi, K. Matsushige, and H. Yamada, Development of low noise cantilever deflection sensor for multienvironment frequency-modulation atomic force microscopy, Rev. Sci. Instrum. **76**, 053704 (2005).

[16] T. Mélin, S. Barbet, H. Diesinger, D. Théron, and D. Deresmes, Note: Quantitative (artifact-free) surface potential measurements using Kelvin force microscopy, Rev. Sci. Instrum. **82**, 036101 (2011).

[17] H. Diesinger and D. Deresmes, Capacitive crosstalk in AM-mode KPFM, in *Kelvin Probe Force Microscopy*, Springer Series in Surface Sciences Vol. 48, edited by Sascha Sadewasser and Thilo Glatzel (Springer, Berlin, Heidelberg, 2012), pp. 25–44.

[18] P. Zahl, T. Wagner, R. Möller, and A. Klust, Open source scanning probe microscopy control software package GXSM, J. Vac. Sci. Technol. B **28**, C4E39 (2010).

[19] J. Melcher, S. Hu, and A. Raman, Equivalent point-mass models of continuous atomic force microscope probes, Appl. Phys. Lett. **91**, 053101 (2007).

[20] T. Glatzel, S. Sadewasser, and M. C. Lux-Steiner, Amplitude or frequency modulation-detection in Kelvin probe force microscopy, Appl. Surf. Sci. **210**, 84 (2003).

[21] T. Hochwitz, A. K. Henning, C. Levey, and C. Daghlian, Capacitive effects on quantitative dopant profiling with scanned electrostatic force microscopes, J. Vac. Sci. Technol. B **14**, 457 (1996).

[22] H. O. Jacobs, P. Leuchtmann, O. J. Homan, and A. Stemmer, Resolution and contrast in Kelvin probe force microscopy, J. Appl. Phys. **84**, 1168 (1998).

[23] E. Strassburg, A. Boag, and Y. Rosenwaks, Reconstruction of electrostatic force microscopy images, Rev. Sci. Instrum. **76**, 083705 (2005).

[24] G. Cohen, E. Halpern, S. U. Nanayakkara, J. M. Luther, C. Held, R. Bennewitz, A. Boag, and Y. Rosenwaks, Reconstruction of surface potential from Kelvin probe force microscopy images, Nanotechnology **24**, 295702 (2013).

[25] A. Labuda, Y. Miyahara, L. Cockins, and P. H. Grütter, Decoupling conservative and dissipative forces in frequency modulation atomic force microscopy, Phys. Rev. B **84**, 125433 (2011).

[26] T. R. Albrecht, P. Grutter, D. Horne, and D. Rugar, Frequency modulation detection using high-Q cantilevers for enhanced force microscope sensitivity, J. Appl. Phys. **69**, 668 (1991).

[27] U. Dürig, H. R. Steinauer, and N. Blanc, Dynamic force microscopy by means of the phase-controlled oscillator method, J. Appl. Phys. **82**, 3641 (1997).

[28] H. Diesinger, D. Deresmes, J.-P. Nys, and T. Mélin, Dynamic behavior of amplitude detection Kelvin force

microscopy in ultrahigh vacuum, Ultramicroscopy **110**, 162 (2010).

[29] W. Denk and D. W. Pohl, Local electrical dissipation imaged by scanning force microscopy, Appl. Phys. Lett. **59**, 2171 (1991).

[30] L. Cockins, Y. Miyahara, S. D. Bennett, A. A. Clerk, S. Studenikin, P. Poole, A. Sachrajda, and P. Grutter, Energy levels of few-electron quantum dots imaged and characterized by atomic force microscopy, Proc. Natl. Acad. Sci. U.S.A. **107**, 9496 (2010).